Chapter 3

Modeling and Simulation of Rotating Machine Windings Fed by High-Power Frequency Converters for Insulation Design

Fermin P. Espino Cortes, Pablo Gomez and Mohammed Khalil Hussain

Additional information is available at the end of the chapter

http://dx.doi.org/10.5772/intechopen.78064

Abstract

Modern power systems include a considerable amount of power electronic converters related to the introduction of renewable energy sources, high-voltage direct current (HVDC) systems, adjustable speed drives, and so on. These components introduce repetitive pulses generated by the commutation of semiconductor switches, resulting in overvoltages with very steep fronts and high dielectric stresses. This phenomenon is one of the main causes of accelerated insulation aging of motors in power electronic-based systems. This chapter presents state-of-the-art computational tools for the analysis of motor windings excited by fast-front pulses related to the use of frequency converters based on pulse-width modulation (PWM). These tools can be applied for the accurate prediction of overvoltages and dielectric stresses required to propose insulation design improvements. In the case of the stress-grading system used in medium-voltage (MV) motors, transient finite-element method (FEM) is used to study the effect of fast pulses. It is shown how, by controlling the material properties and the design of the stress-grading systems, solutions to reduce the adverse effects of fast pulses from PWM-type inverters can be proposed.

Keywords: dielectric stress, fast-front pulses, motor windings, pulse-width modulation

1. Introduction

The detrimental effect of steep voltage surges propagating along the windings of power components such as transformers, reactors, motors, generators, and so on has been a topic of great interest for almost a century (see for instance [1–6]). In the case of motors, these surges

have been traditionally associated with energization, re-energization, or incoming lightning pulses [7]. Over the last decades, this has become a larger issue with the increasing use of frequency converters for speed and torque control, which introduce repetitive steep-front voltage impulses and associated partial discharges into the machine windings (see **Figure 1**). The insulation of this type of devices is subjected to high and sustained electric and thermal stresses [8, 9]. This effect is further amplified by the use of long connection cables [10].

Industrial surveys and other studies show that 20–40% of rotating machine failures are due to stator winding problems, and 70% of these are due to insulation failures [11–16]. Dielectric stress along motor's windings associated with the propagation of fast-front voltage surges is a major source of premature deterioration or failure of the insulation system of these devices [9, 17].

Early motor representations for fast-transient studies consisted of approximating the surge impedance of the motor as a simple lumped termination of the feeding cable [18]. This allowed understanding and predicting the transient overvoltages produced at the cable/motor connection. However, overvoltages can appear at several points inside the machine coils during the transient period. Models that are more detailed were later introduced to consider the transient potential distribution along windings. These models are known as white box models and can be classified in lumped and distributed parameter representations [7]. Although the former are easier to implement and less computationally expensive, the latter are more accurate since the wave propagation along the winding coils is introduced in a more precise manner.

Rudenberg first introduced the application of traveling wave theory to study the fast-transient behavior of windings [19]. A more rigorous approach based on a multi-conductor line model and applied to transformer windings was described by Rabins in 1960 [20]. Oraee [4] and Guardado [5] independently developed this approach for electrical machines in the 1980s. The main idea of their modeling approach is that a coil can be approximated by a multi-conductor transmission line (MTL): each conductor represents a turn (or group of turns) of the coil, and the continuity between the end of one turn and the beginning of the next one is preserved by

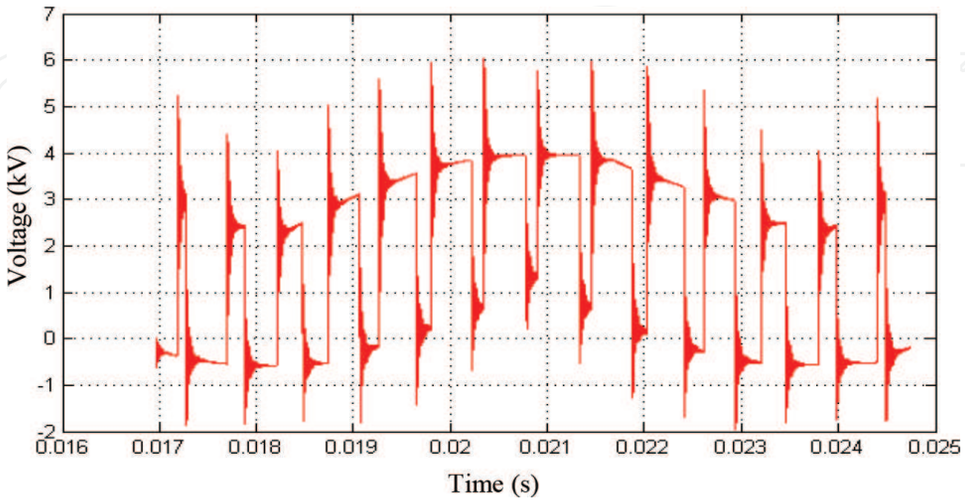

Figure 1. Typical voltage to ground of a medium-voltage winding fed by a three-level converter.

http://dx.doi.org/10.5772/intechopen.78064

means of a topological connection between the corresponding nodes. This is called a zig-zag connection and is shown in **Figure 2**.

The distributed parameter model of an MTL is completely characterized by its electrical parameter matrices: series impedance matrix **Z** and shunt admittance matrix **Y**. For the case of machine windings, these matrices are obtained from the geometrical configuration of the machine. Considering the typical stator coil diagram depicted in **Figure 3**, the incident surge

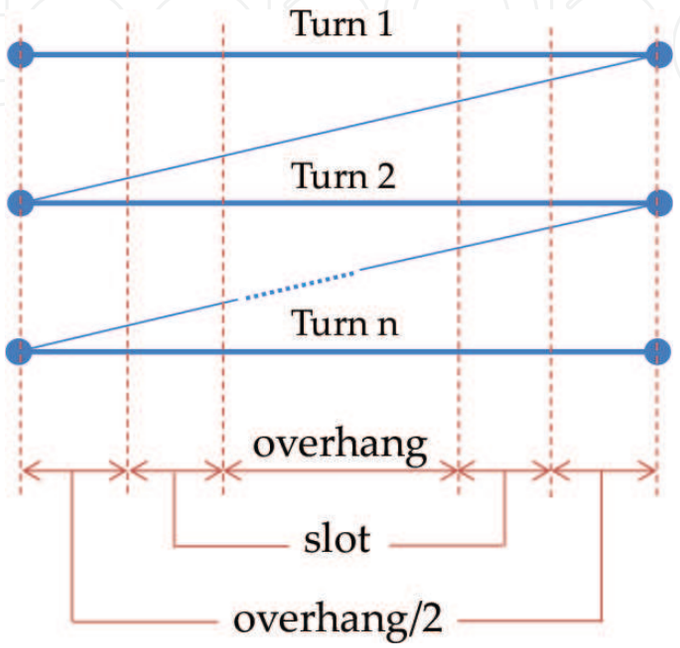

Figure 2. Multi-conductor transmission line model of the coil with a zig-zag connection (three turns are considered for the purpose of illustration) [21].

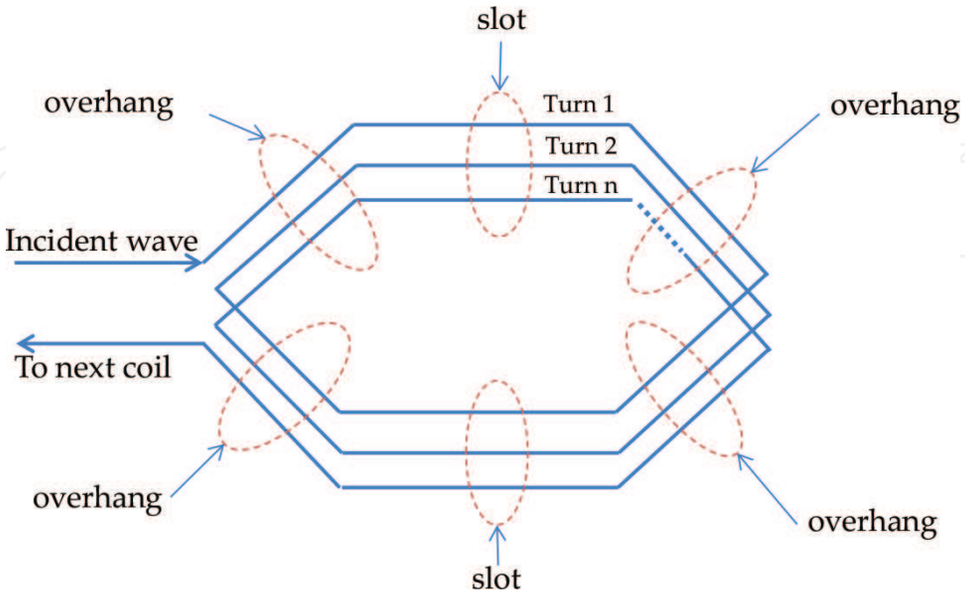

Figure 3. Coil sections in the stator frame [21].

will propagate along two different regions: slot and overhang. Due to the variation in the electromagnetic field distribution in these two regions, the corresponding parameter matrices will also be different [5].

Another challenging aspect of machine-winding modeling is the computation of electrical parameters. Common approaches followed for this task are (1) measuring the parameters, (2) applying analytical expressions, and (3) applying numerical methods. Analytical and numerical methods are the only possible choices for new designs. However, since machine windings have complex geometrical features, the available analytical expressions rely on numerous approximations and assumptions and are therefore restricted to particular geometries. Numerical methods are applicable in a more general sense as long as detailed geometrical and electrical data are available, which is the case at the design stage [22].

One of the first insulation problems stemming from the use of power frequency converters with medium-voltage (MV) motors was associated with the electric stresses on the surface of the coils. Partial discharge (PD) and heat can erode the coatings of the stress-grading (SG) system [23], aggravating the problem and, perhaps, eventually destroying the ground-wall insulation. This process can take a long time to produce a critical failure, but the ozone produced as a byproduct of surface PD [24] may accelerate the degradation and hence the need to rewind the motor [23].

The SG system in MV-rotating machines is composed of two coatings: the conductive armor coating and the semi-conductive stress-grading coating. The conductive armor coating is a relatively conductive layer that is usually applied in the form of a tape to the surface of the ground-wall insulation in form-wound coils that lies inside the stator slot of a rotating machine. The function of this coating is to limit the surface potential of the coil to a value equal or close to ground potential, thereby avoiding the possibility of discharges between the coil insulation and the slot wall. The length of the conductive armor coating extends beyond the end of the slot [25], as illustrated by part A in **Figure 4**. The semi-conductive-grading coating starts at the end of the conductive armor coating, part B, also in the form of a tape, and they are often overlapped by a couple of centimeters, shown as region E. The purpose of the semi-conductive-grading coating is to produce a smooth transition from the potential in the conductive armor coating to the high voltage (HV) on the surface of the coil insulation outside of the slot, shown as part C in **Figure 4**. The graded voltage drop along the surface of the coil avoids harmful high electric field concentrations.

The conductive armor coating is commonly a composite of either varnish or polyester resin filled with graphite or carbon black. It is considered as a constant conductivity layer with values between 10 and 0.01 S/m. The semi-conductive-grading coating of coils is a composite of silicon carbide (SiC) and varnish or polyester resin, with a field-dependent conductivity. A profile of the voltage from the slot exit to the end of the semi-conductive-grading tape (SGT) measured using an alternating current (AC) electrostatic voltmeter is shown in **Figure 5**. The coil was energized with 8 kVrms at 60 Hz. The conductive armor tape (CAT) is at ground potential (first 10 cm in the plot of **Figure 5**) while along the SGT the voltage increases smoothly (after 10 cm), something that is accomplished by the generation of resistive heat as

http://dx.doi.org/10.5772/intechopen.78064

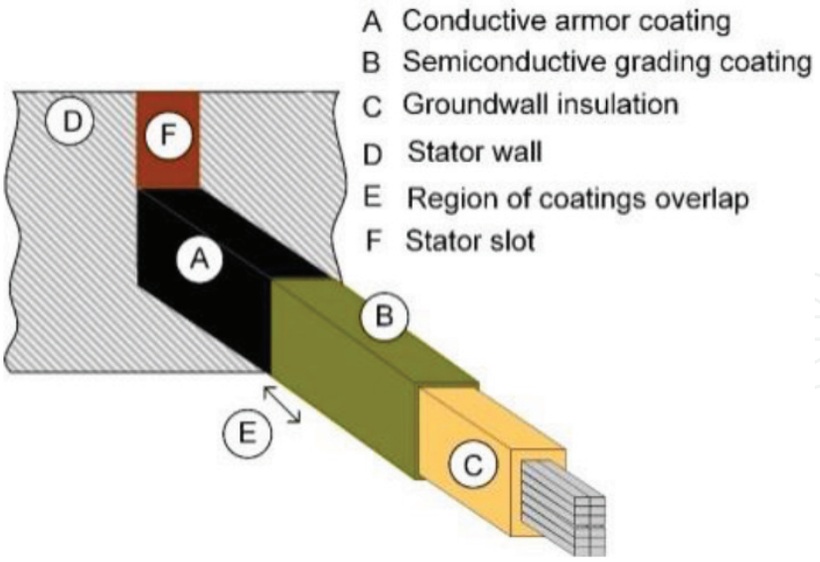

Figure 4. Illustration showing conductive armor and semi-conductive-grading coatings on a form-wound coil [26].

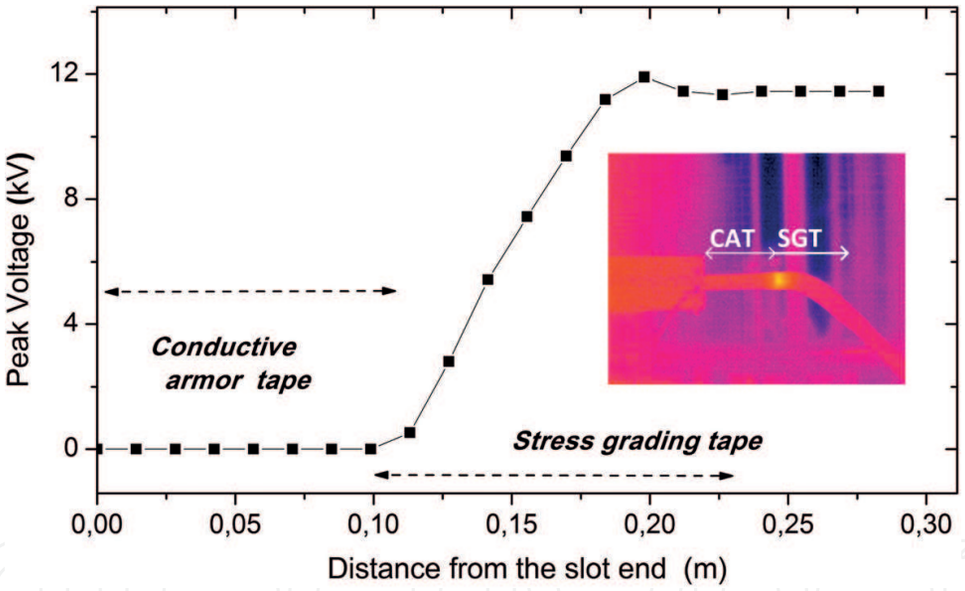

Figure 5. Illustration showing conductive armor and stress-grading coatings on a form-wound coil under sinusoidal 60-Hz voltage [26].

seen in the inserted infrared image of **Figure 5**, where the section of the SG presents a hot spot. The slope of the voltage defines the tangential electric field on the surface of the stress-grading region. Overvoltages and pulses having steep fronts, like those from PWM-type inverters, considerable modify the stress relief in the SGT and in the portion of the CAT that is outside of the slot. The design of the stress grading and the conductive armor coatings has become difficult under this condition, and modeling had resulted in a useful tool in understanding the influence of the various design parameters.

The remaining of this chapter is divided as follows: Section 2 describes the modeling and parameter determination of motor windings excited by the fast pulses produced by an inverter. Section 3 describes a finite-element method (FEM)-based approach to analyze the performance of stress-grading systems. Finally, Section 4 presents the conclusions and final remarks of this chapter.

2. Fast-transient modeling of rotating machine windings for inverter excitation

The computer model described in this section for the prediction of the fast-transient response of the machine winding is a non-uniform, multi-conductor, distributed-parameter model defined in the frequency domain. This model is selected over other alternatives given its good balance between high accuracy and practicality, as explained below:

1. *Why non-uniform?* The distribution of electric and magnetic fields is different in the slot and overhang regions, resulting in different electrical parameters for each region that should be considered to accurately reproduce the pulse propagation. In this case, the non-uniform model consists of five segments considering the typical geometry of a wound-form motor, as shown in **Figures 3** and **6**.
2. *Why multi-conductor?* This modeling approach of the winding allows natural inclusion of the inductive and capacitive coupling between turns [21].
3. *Why based on distributed parameters?* A distributed parameter model based on transmission line theory can represent the propagation of a fast pulse along windings in a more rigorous manner than a lumped parameter model based on circuit theory [27].
4. *Why defined in the frequency domain?* The partial differential equations describing wave propagation in time domain become ordinary differential equations in the frequency domain, making the solution more straightforward. In addition, including frequency dependence of the system parameters is substantially easier in the frequency domain than in the time domain [28].

The winding electrical parameters (capacitance, inductance, and losses) in the overhang and slot regions of the coil are calculated using the finite-element method (FEM)-based software COMSOL Multiphysics [29], as described in Section 2.2.

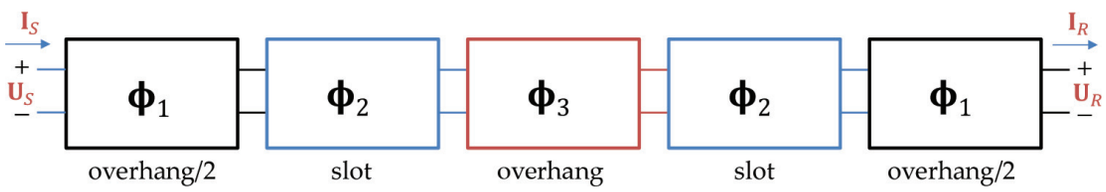

Figure 6. Cascaded connection of chain matrices to model all coil regions [22].

http://dx.doi.org/10.5772/intechopen.78064

2.1. Winding model

Wave propagation along the non-uniform multi-conductor transmission system representing the winding is defined by the Telegrapher equations in the Laplace domain as follows [30, 31]:

$$\frac{d}{dx}\begin{bmatrix}\mathbf{U}(x,s)\\ \mathbf{I}(x,s)\end{bmatrix}=\begin{bmatrix}0 & -\mathbf{Z}(x,s)\\ -\mathbf{Y}(x,s) & 0\end{bmatrix}\begin{bmatrix}\mathbf{U}(x,s)\\ \mathbf{I}(x,s)\end{bmatrix} \tag{1}$$

In Eq. (1), $\mathbf{U}(x,s)$ and $\mathbf{I}(x,s)$ are the voltage and current vectors at point x along the line, $\mathbf{Z}(x,s)$ and $\mathbf{Y}(x,s)$ are the series impedance and shunt-admittance matrices of the line per unit length, respectively. According to Eq. (1), the winding electrical parameters are a function of both space and time. Voltages and currents at the terminals of the segment can be related using the chain matrix definition, assuming constant parameters over a segment Δx and applying boundary conditions at x and $x + \Delta x$ [31]:

$$\begin{bmatrix}\mathbf{U}(x+\Delta x,s)\\ \mathbf{I}(x+\Delta x,s)\end{bmatrix}=\boldsymbol{\phi}(\Delta x,s)\begin{bmatrix}\mathbf{U}(x,s)\\ \mathbf{I}(x,s)\end{bmatrix} \tag{2}$$

where the chain matrix of the segment is defined as

$$\boldsymbol{\phi}(\Delta x,s)=\begin{bmatrix}\cosh(\boldsymbol{\psi}\Delta x) & -\mathbf{Y}_0^{-1}\sinh(\boldsymbol{\psi}\Delta x)\\ -\mathbf{Y}_0\sinh(\boldsymbol{\psi}\,\Delta x) & \mathbf{Y}_0\cosh(\boldsymbol{\psi}\Delta x)\mathbf{Y}_0^{-1}\end{bmatrix} \tag{3}$$

In Eq. (3), $\boldsymbol{\psi}$ is the propagation constant matrix of the line, given by $\boldsymbol{\psi}=\mathbf{M}\sqrt{\boldsymbol{\lambda}}\mathbf{M}^{-1}$, where $\mathbf{M}$ and $\boldsymbol{\lambda}$ are the eigenvalue and eigenvector matrices of the $\mathbf{Z}(x,s)\mathbf{Y}(x,s)$ product, respectively. In addition, $\mathbf{Y}_0$ is the characteristic admittance matrix of the line segment, given by $\mathbf{Y}_0=\mathbf{Z}(x,s)^{-1}\boldsymbol{\psi}$. The two-port representation defined by Eq. (2) is the basis of the non-uniform model of the machine-winding coil, according to the following procedure [21]:

1. The coil is divided into five segments, as shown in **Figures 2** and **6**.
2. Each of the five chain matrices is obtained from Eq. (3) as a function of parameters **Z** and **Y**, which are different in the geometrical regions identified as overhang and slot.
3. The chain matrices are multiplied according to the cascaded connection shown in **Figure 6** in order to obtain a single chain matrix representing the complete coil.

Voltages and currents at the sending (S) and receiving (R) nodes of the complete coil are related as follows:

$$\begin{bmatrix}\mathbf{U}_R\\ \mathbf{I}_R\end{bmatrix}=\boldsymbol{\phi}_1\boldsymbol{\phi}_2\boldsymbol{\phi}_3\boldsymbol{\phi}_2\boldsymbol{\phi}_1\begin{bmatrix}\mathbf{U}_S\\ \mathbf{I}_S\end{bmatrix}=\begin{bmatrix}\boldsymbol{\Phi}_{11} & \boldsymbol{\Phi}_{12}\\ \boldsymbol{\Phi}_{21} & \boldsymbol{\Phi}_{22}\end{bmatrix}\begin{bmatrix}\mathbf{U}_S\\ \mathbf{I}_S\end{bmatrix} \tag{4}$$

In Eq. (4), $\boldsymbol{\Phi}_{11}$, $\boldsymbol{\Phi}_{12}$, $\boldsymbol{\Phi}_{21}$, and $\boldsymbol{\Phi}_{22}$ are the elements of the complete chain matrix representation of the coil. This representation is transformed into an equivalent admittance matrix form to

include the zig-zag connection in order to preserve continuity between turns as a pulse propagates along the coil (see **Figure 2**) [32, 33]. This yields

$$\begin{bmatrix} \mathbf{U}_S \\ \mathbf{U}_R \end{bmatrix} = \begin{bmatrix} \mathbf{Y}_{SS} + \mathbf{Y}_{con11} & -(\mathbf{Y}_{SR} + \mathbf{Y}_{con12}) \\ -(\mathbf{Y}_{SR} + \mathbf{Y}_{con21}) & \mathbf{Y}_{RR} + \mathbf{Y}_{con22} \end{bmatrix}^{-1} \begin{bmatrix} \mathbf{I}_S \\ \mathbf{U}_R \end{bmatrix} \tag{5}$$

The admittance matrix and chain matrix elements are related according to the following expressions:

$$\mathbf{Y}_{ss} = -\mathbf{\Phi}_{12}^{-1}\mathbf{\Phi}_{11}, \mathbf{Y}_{SR} = -\mathbf{\Phi}_{12}^{-1} = -\mathbf{\Phi}_{22}\mathbf{\Phi}_{12}^{-1}\mathbf{\Phi}_{11} + \mathbf{\Phi}_{21}, \mathbf{Y}_{RR} = -\mathbf{\Phi}_{22}\mathbf{\Phi}_{12}^{-1} \tag{6}$$

In Eq. (5), admittance submatrices $\mathbf{Y}_{con11}$, $\mathbf{Y}_{con12}$, $\mathbf{Y}_{con21}$, and $\mathbf{Y}_{con22}$ are included to connect the end of each turn to the beginning of the next one (zig-zag connection), as well as the source and load admittances representing winding terminal connections.

The Laplace-domain voltages at each turn of the coil are obtained from Eq. (5). These voltages are finally transformed into transient voltage responses in the time domain by means of the application of the inverse numerical Laplace transform [28].

2.2. Parameter computation

FEM-based simulation program COMSOL Multiphysics is used to compute the capacitance and inductance matrices in the overhang and slot regions of the machine winding [29]. For the calculation of inductance in the slot region, it is assumed that the slot walls behave as magnetic insulation due to eddy currents at the high frequencies related to the pulses produced by frequency converters, meaning that the flux is normal to the boundary and does not penetrate the core. In the overhang region, these walls are replaced by an open-boundary condition.

2.2.1. Capacitance

Capacitance matrix **C** is calculated using the electrostatics module of COMSOL using the forced voltage method as follows [22]:

$$\begin{bmatrix} Q_1 \\ \vdots \\ Q_n \end{bmatrix} = \begin{bmatrix} C_{11} & \cdots & C_{1n} \\ \vdots & \ddots & \vdots \\ C_{n1} & \cdots & C_{nn} \end{bmatrix} \begin{bmatrix} U_1 \\ \vdots \\ U_n \end{bmatrix} \tag{7}$$

The charge in all n elements due to conductor i is obtained by exciting conductor i with a fixed voltage while defining all other conductors at zero potential, thus obtaining the i-th column of the capacitive matrix. This process is repeated for each conductor to obtain the complete matrix.

2.2.2. Inductance

Inductance matrix **L** is computed from the magnetic energy method [22]. The current is nonzero in one or two terminals at a time and the energy density is integrated over the whole

http://dx.doi.org/10.5772/intechopen.78064

geometry. Self-inductance L_{ii} is obtained from the magnetic energy $W_{m,i}$ due to the injection of a current I_i to turn i:

$$L_{ii} = \frac{2W_{m,i}}{I_i^2} \tag{8}$$

Mutual inductance L_{ij} is obtained from the magnetic energy $W_{m,ij}$ due to the simultaneous injection of current to turns i and j:

$$L_{ij} = \frac{W_{m,ij}}{I_i I_j} - \frac{1}{2}\left(\frac{I_i}{I_j}L_{ii} + \frac{I_j}{I_i}L_{jj}\right) \tag{9}$$

When using this method, all self inductances must be computed first and then applied for the computation of mutual inductances.

2.2.3. Losses

The series losses matrix (**R**) of the winding is considered frequency-dependent and obtained from the concept of complex penetration depth [22]. The dielectric losses matrix (**G**) is computed using the "electric currents" module in COMSOL [29]. Finally, the series impedance and shunt admittance matrices required by the winding model are computed according to $\mathbf{Z} = \mathbf{R} + s\mathbf{L}$ and $\mathbf{Y} = \mathbf{G} + s\mathbf{C}$.

2.3. Case study

A schematic cross-section of the coil considered in this study is shown in **Figure 7**. The main parameters of the stator coil are summarized in **Table 1**. **Figure 8** shows a schematic representation and a picture of the experimental setup. Besides the MV form-wound coil under test, it includes a waveform generator (Keysight 33500B), an oscilloscope (Agilent DSO-X 2014A), and a 100-Ω load connected at the end of the coil. Steel plates were included to emulate the EM field distribution in the slot region [34]. The experimental setup was placed in a laboratory facility free of EM interference. More details of this test case can be found in [35].

The capacitance and inductance matrices are computed from FEM simulations using COMSOL Multiphysics, as explained in Section 2.2. Sample simulations are shown in **Figures 9** and **10** for the first turn.

Figure 9 shows the distribution of electric potential when turn 1 (top turn) is excited with 1 V, while all other turns and the slot walls are grounded. This allows the calculation of the first column of the capacitance matrix of the coil using Eq. (7). **Figure 10** shows the distribution of magnetic energy density when turn 1 is excited with 1 A, while all other turns are left unexcited. Integrating this magnetic energy density results in the magnetic energy required in Eq. (8) to compute the self-inductance of turn 1.

The winding model is validated considering a PWM-type excitation with different rise times between 100 and 500 ns connected to the first turn of the coil. The rest of winding is represented

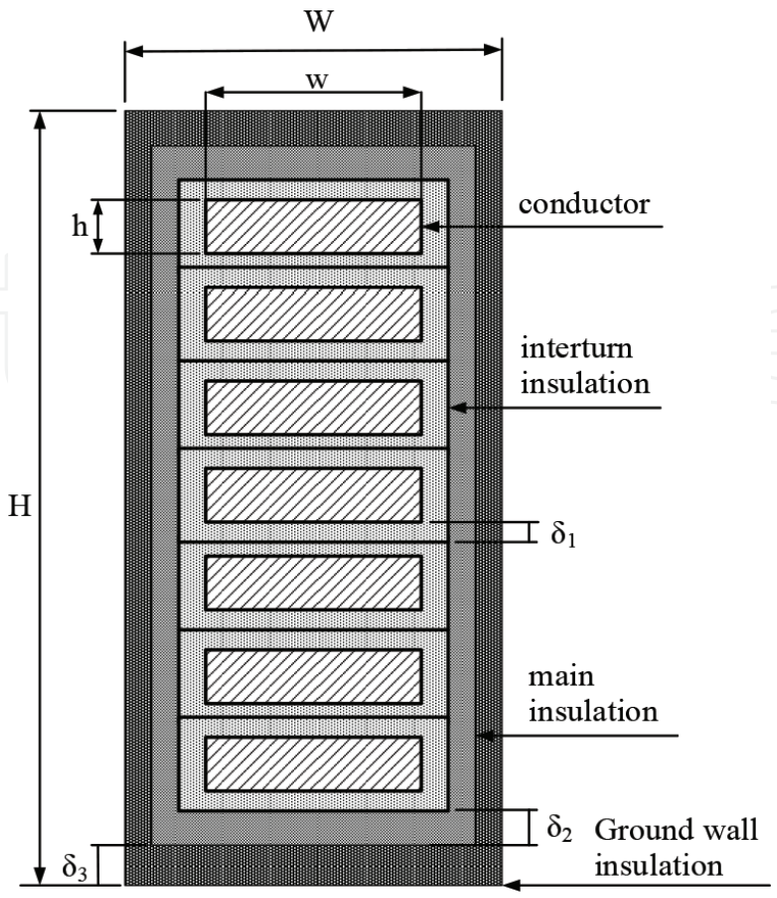

Figure 7. Cross section of the coil with three insulation layers [35].

Turns per stator coil	7
Length of overhang region	0.33 m
Conductor width (w)	5.35 mm
Conductor height (h)	2.85 mm
Resistivity of stator bar conductor	1.7×10^{-8} Ω·m
Thickness of interturn insulation (δ1)	0.2 mm
Thickness of main insulation (δ2)	1.41 mm
Thickness of ground-wall insulation (δ3)	0.36 mm
Relative permittivity of the interturn insulation	2.5
Relative permittivity of the main insulation	2
Relative permittivity of the ground-wall ins	2.8
Slot width (W)	8.9 mm
Slot height (H)	24.2 mm
Slot length	0.45 m

Table 1. Rotating machine parameters [35].

http://dx.doi.org/10.5772/intechopen.78064

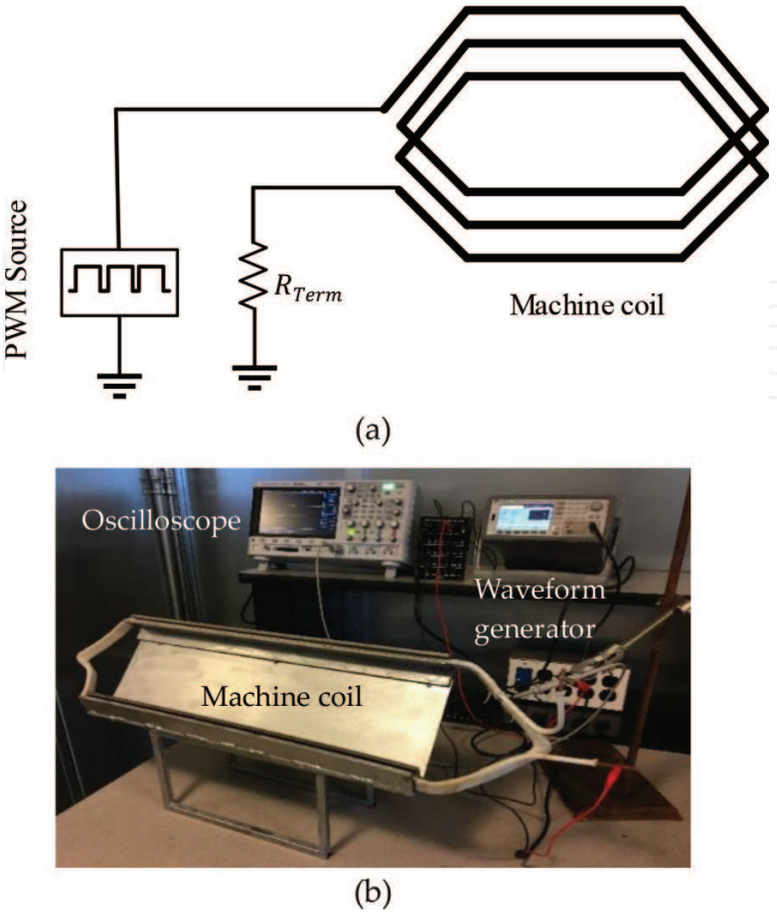

Figure 8. Experimental setup for validation of the inverter-coil setup: (a) schematic diagram showing main parts and (b) photography of laboratory components [35].

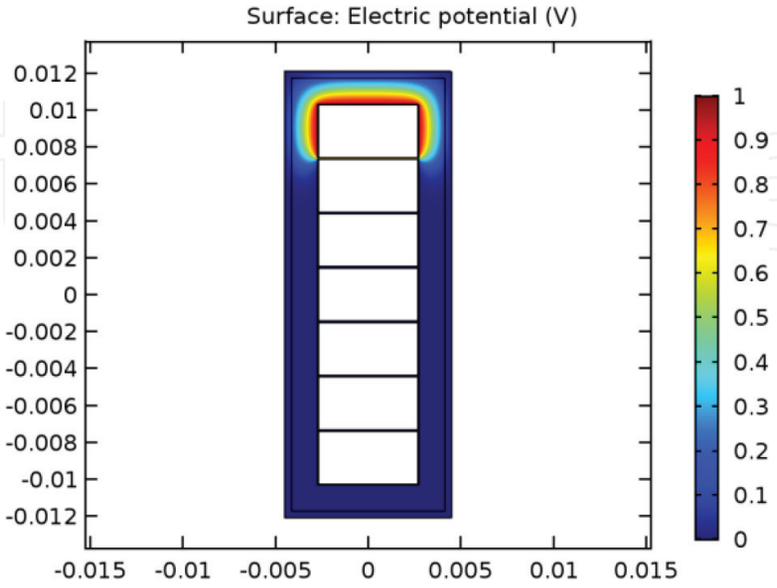

Figure 9. Capacitance calculation using forced voltage method in FEM [35].

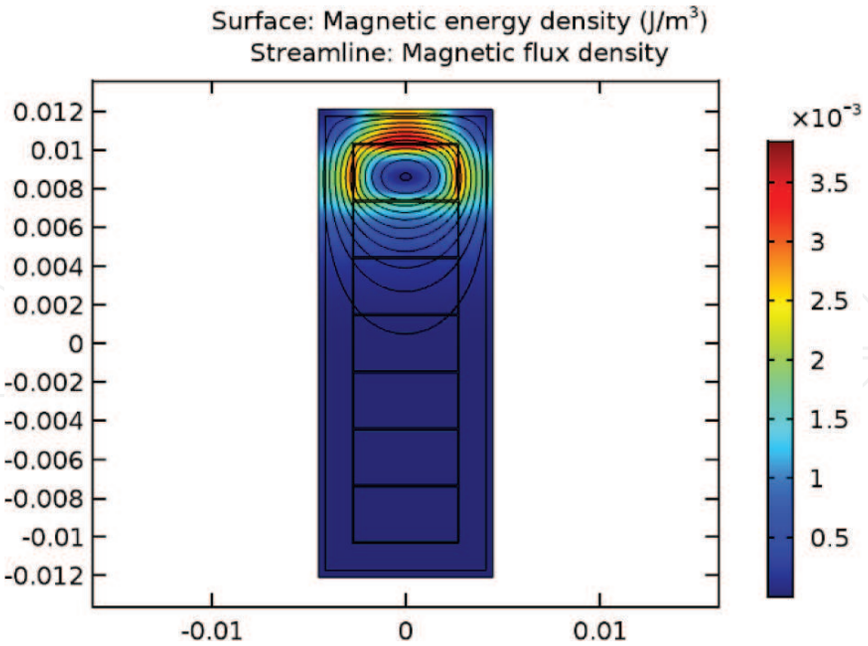

Figure 10. Inductance calculation using magnetic energy method in FEM [35].

by a 100-Ω load. This type of excitation is obtained from the waveform generator emulating the phase-to-ground voltage from a voltage source inverter.

Figure 11 shows the comparison of the simulated and measured transient voltage at the first winding turn for excitations with different rise times. It can be noticed that the magnitude of the overshoot produced depends on the rise time of the excitation. A second assessment of the winding corresponds to a similar setup, but with an open-ended condition of the coil. This results in noticeable oscillations, which are reproduced in a very accurate manner by the winding model, as shown in **Figure 12**, which illustrates the transient response at the far end

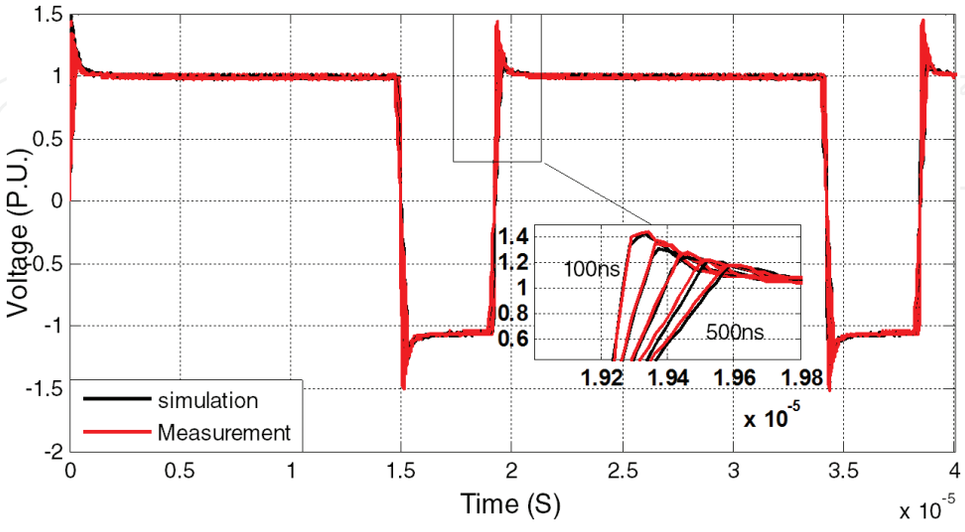

Figure 11. Transient overvoltage at the first turn of the coil terminated in 100-Ω load [35].

http://dx.doi.org/10.5772/intechopen.78064

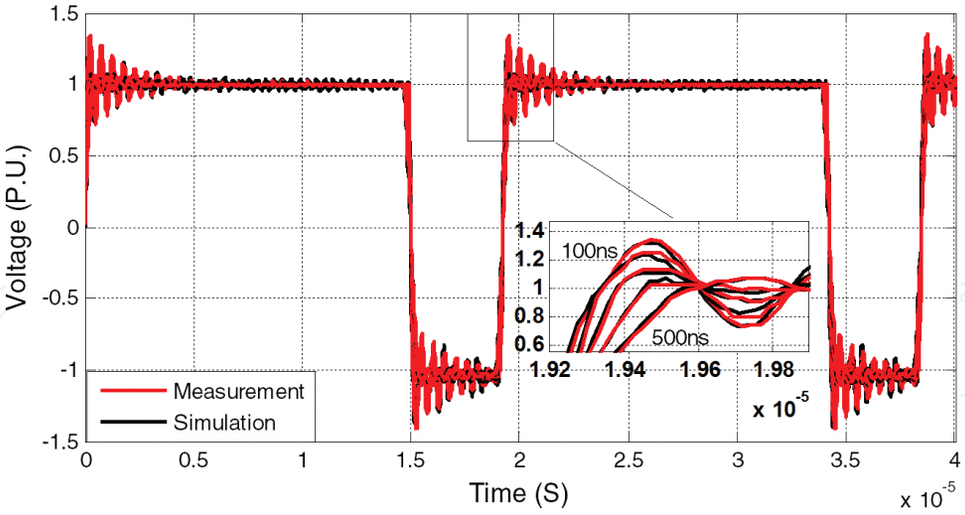

Figure 12. Transient overvoltage at the last turn of the coil for open-ended case [35].

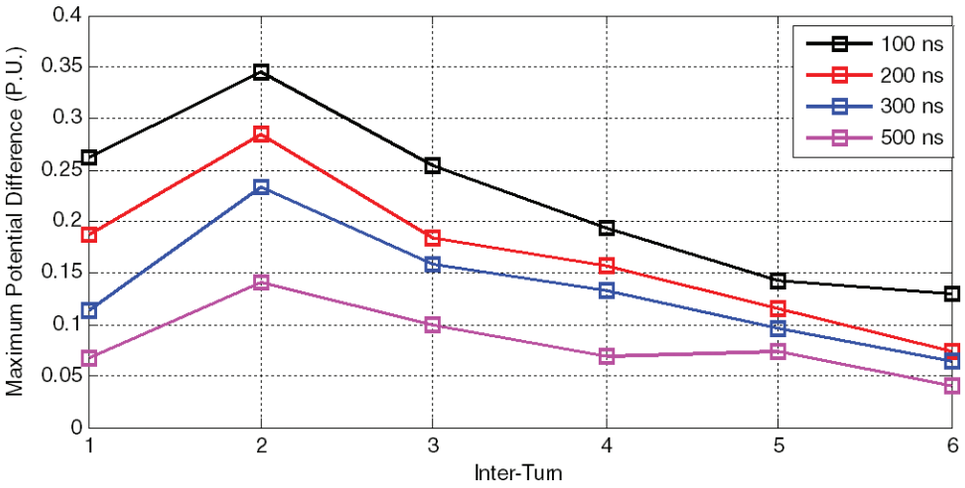

Figure 13. Potential difference between turns considering different rise times of the excitation [35].

of the winding. As in the previous case, the maximum overvoltages are related to the highest rise time of the excitation.

The effect of the excitation rise time is analyzed in a more general manner in **Figure 13**, which shows the potential difference between turns for different rise times. According to this figure, the potential difference is inversely proportional to the rise time of the excitation.

3. Modeling of stress-grading systems from rotating machines

Modeling of stress-grading systems of MV rotating machines is an essential tool for their design and optimization. An accurate model can serve several purposes, such as [36]:

1. describing how the system is likely to behave under certain conditions;

2. modifying the material characteristics to match specific requirements;
3. predicting the effects of aging and determining the material's life time in order to establish a maintenance policy.

FEM has become one of the most commonly used techniques for modeling stress-grading systems [37–39]. With FEM, the geometry can be considered including most of the details that influence the electric field distribution. To determine how the electric field stress is distributed during PWM voltage excitation, the problem must be solved in the time domain with considerably small time steps. This, together with the high nonlinearity of the semi-conductive stress-grading coating, makes modeling of SG systems a complicated task [40, 41].

3.1. Modeling of stress-grading systems

In the general case, problems with stress-grading systems can be represented with subdomains of conductors, subdomains of perfect dielectrics (air or another surrounding medium and main insulation), and subdomains of stress-grading materials [42]. Conductors can be considered perfect conducting regions of known potential. Neglecting the dielectric loss component of the materials, the equation to be solved is of the form [43]

$$\nabla\cdot[-\sigma(\mathbf{E})\nabla U] + \frac{\partial[\nabla\cdot(\varepsilon_r\varepsilon_0(-\nabla U))]}{\partial t} = 0 \tag{10}$$

where σ is the electrical conductivity, ε_r is the relative permittivity, and ε_0 is the vacuum permittivity. The electric field dependency ($\sigma(\mathbf{E})$) of the semi-conductive-grading coating helps to limit the maximum electric field on the surface of the coil giving adaptability to different designs and voltage levels [44]. For proper FEM simulations, it is required to know the nonlinearity of the electrical conductivity at high electric stress for the semi-conductive-grading material. One of the most common expressions used to define the electric field dependency in S/m of this coating is given by [45, 46]

$$\sigma(E_t) = \sigma_0 \exp(\alpha {E_t}^n) \tag{11}$$

where σ_0 = 1.85 x 10^{-9} S/m, α= 0.00112, and n = 0.67. Eq. (10) can be solved analytically or numerically. FEM or an Equivalent Electric Circuit Model [36] can be used for this purpose. FEM is widely used to model the SG coatings due to some advantages over, for example, equivalent circuit models. With circuit models, some geometric aspects of the SG systems, like overlapping of coatings or the sharp end of the slot exit, are difficult to be considered. In addition, with FEM, the thermal field problem can be solved using the same geometry, taking as a source of heat the ohmic losses from the electric solution.

Transient FEM with efficient algorithms needs to be used in order to solve the highly nonlinear problem associated with SG coatings. Nowadays, FEM software provides new capabilities that allow performing highly nonlinear simulations. The "electric currents" module of the FEM-based software COMSOL Multiphysics [29] is used in the next sections to compute the electric

http://dx.doi.org/10.5772/intechopen.78064

field distribution and resistive heat produced in the CAT and SGT of form-wound coils under the application of fast rise time pulses.

3.2. FEM modeling of stress-grading coatings under PWM voltage waveforms

With the aid of an infrared camera, it is possible to observe the heat generated because of the electric stress grading under fast pulses. In order to show this condition, a 4.2-kV form wound coil was energized with 4-kV squared pulses with a repetition rate of 2000 pulses per second, and the temperature was registered using an infrared camera model Flir-SC500. As it can be seen in **Figure 14**, the heat distribution is different in comparison to that presented in **Figure 5** for power frequency (60 Hz); under this condition, the high electric stress moves from the SGT to the CAT at slot exit. Something important to notice in the infrared image is the presence of hot spots that follow the patterns of the CAT tapping; this will be discussed in Section 3.4.

Usually, modeling of the conductive armor coating and the semi-conductive-grading coatings is done separately; however, under fast pulses, it is important to understand the combined performance of both coatings. Therefore, the analysis of coil ends working with PWM voltages requires the simultaneous simulation of both coatings.

3.2.1. Finite-element dimension reduction on the stress-grading coatings

A useful tool in FEM modeling is the ability of reducing the dimension of the elements used to discretize the stress-grading coating subdomain [29]. These coatings are applied in thin layers that require a very fine element discretization; otherwise, if a coarse discretization of the subdomains is used, numerical instability may result [47]. Assuming that the conductivity of the semi-conductive coating depends only on the tangential component of the electric field, the elements used in the SG coatings can be reduced to one dimension (1D) [48]. If the geometry of the problem is considered in two dimensions (2D), as shown in **Figure 15(a)**, the subdomains

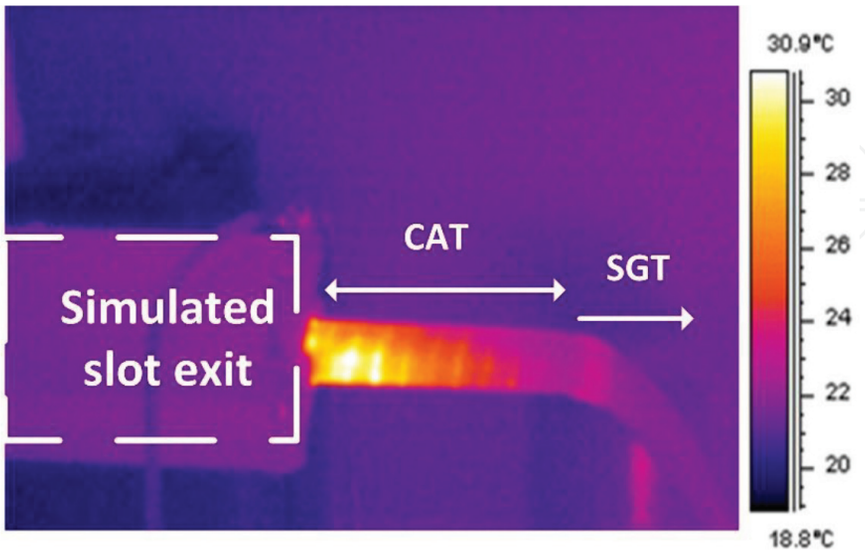

Figure 14. Temperature profile on a 4.2-kV coil end under 650-ns rise time pulses with a repetition rate of 2000 pulses per second. Peak voltage: 4.0 kV [26].

for the CAT and SGT can be discretized using one-dimensional elements (electric shielding boundary in COMSOL), thereby considerably reducing the total number of elements and, in most cases, making it easier for the solution to converge.

Consider for simulation the 2D geometry of the coil end shown in **Figure 15(a)** and the transient voltage of a leading edge of one PWM pulse, shown in **Figure 15(b)**. The pulse has a rise time of 1 μs and an overshoot of around of 1.6 times the nominal phase to ground peak voltage for a 6.6-kV coil. The thickness of the ground-wall insulation is 3 mm, the CAT and SGT are 0.5 mm thick, and their lengths are 50 and 100 mm, respectively. The CAT conductivity is 0.01 S/m, and the conductivity of the SGT is given by Eq. (11). The relative permittivities (ε_r) of the CAT and the SGT are, respectively, 50 and 20. A comparison of the results for the electric field on the CAT and SGT using 1D and 2D elements is presented in **Figure 16**. As it can be seen in this figure, this 1D simplification does not modify the results when compared to the solution obtained considering 2D elements.

In addition, the simplification from a 2D to a 1D modeling can be indeed useful, especially when non-axial-symmetric geometries need to be modeled in three dimensions. For example, form-wound coils can be modeled in 3D, when considering 2D elements in the stress-grading subdomains [49]. One problem that occurs with this simplification is that geometrical details like overlapping in multilayer systems are sometimes difficult to implement.

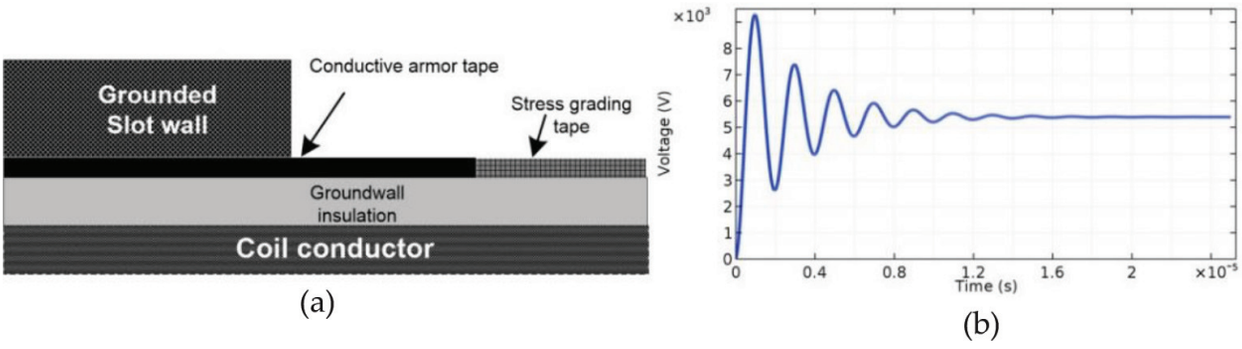

Figure 15. (a) Cross-section illustration of the form-wound coil and (b) transient pulse voltage waveform considered in the transient FEM simulations [26].

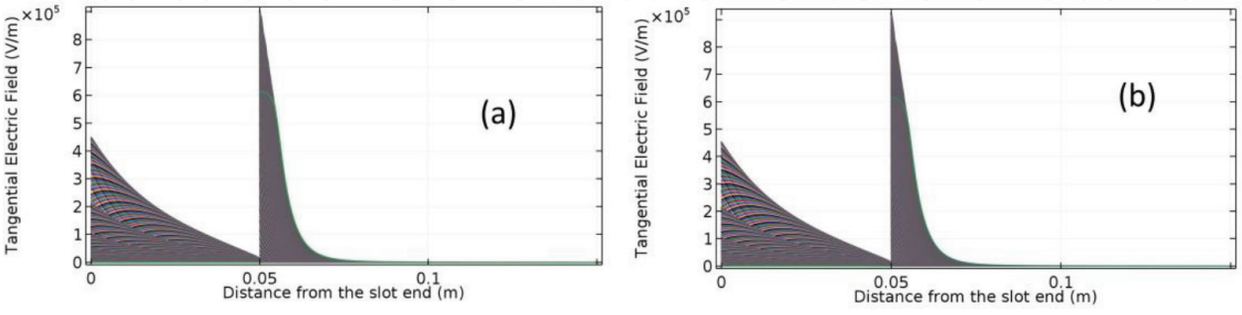

Figure 16. Tangential electric field distribution along the stress-grading coatings computed using (a) 2D elements and (b) 1D elements.

http://dx.doi.org/10.5772/intechopen.78064

However, simulations using discretization of the CAT and SGT with one dimension elements reduction can give a sufficiently good approximation when these details are not required in the simulations.

When the response of an SG system during a PWM waveform needs to be modeled, a large computing time is generally required, since the time step is defined by the fast rise time of the pulses (1 μs or less) and the simulation time is in the order of several milliseconds. Using reduced dimension elements in the CAT and SGT domains makes the simulation computationally more efficient. One example of the convenience of this dimension reduction is shown with the transient simulation of electric field and heat in a coil with 3-mm thickness of the ground-wall insulation, and 1 mm CAT and SGT thickness; the length of the CAT is 50 mm from the slot exit. The CAT conductivity is 0.01 S/m, and the relative permittivity is 100. The length of the SGT is 100 mm. The SGT has a relative permittivity of 20 and a nonlinear conductivity given by Eq. (11). Considering a phase-to-ground three-level PWM voltage [50], which waveform is shown in the inset of **Figure 17(a)**, the magnitude of the tangential electric stress versus time is present along both coatings, as it can be observed in **Figure 17(a)**. The magnitude of the resistive heat density along the CAT and SGT as a function of time and electric field is presented in **Figure 17(b)**. According to this figure, the heat is concentrated mainly in the CAT.

The tangential component of the electric field in the CAT is well below the tangential electric field in the SGT (**Figure 17(a)**), but the heat generated in this coating is considerably higher (**Figure 17(b)**). Experimental work on form-wound coils stressed by fast pulses has shown that this condition can damage the CAT, allowing surface PD to appear right at the slot exit [51, 52]. The next section introduces the use of FEM modeling to investigate possible solutions to this problem.

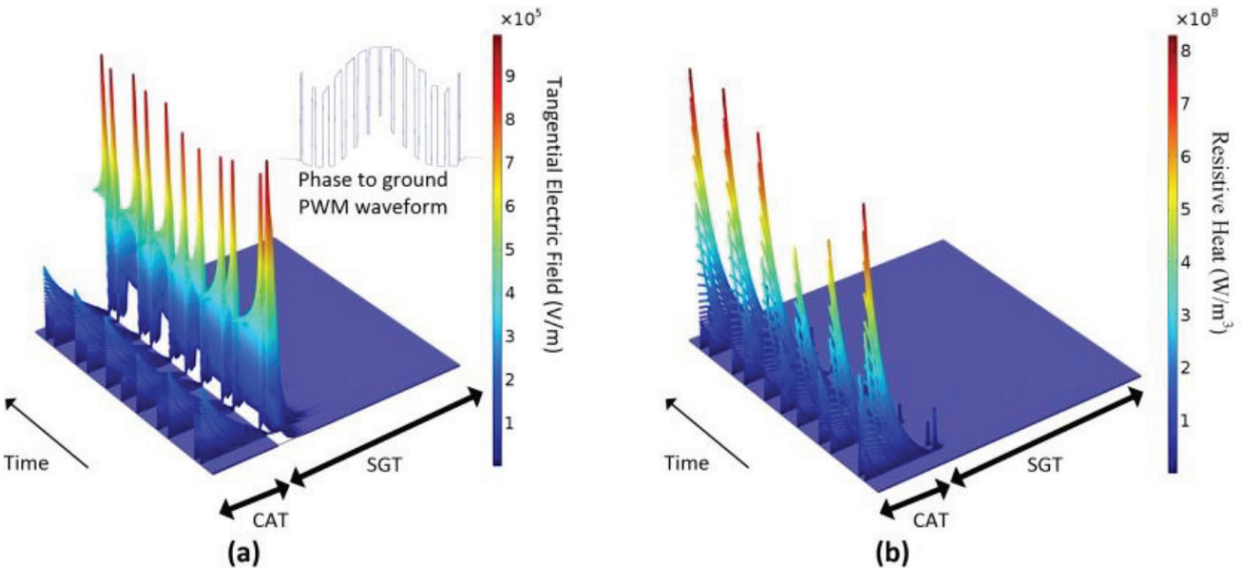

Figure 17. (a) Tangential electric field distribution along the surface from the slot end of the coil under a phase to ground PWM waveform and (b) resistive heat [53].

3.3. Modeling for the design of stress-grading coatings under PWM voltages

As mentioned before, the SG systems in motor coil ends can fail because of the excessive heat generated when they operate under fast rise time pulses like those produced by adjustable speed drives. The excessive heat produced in the CAT can be considered the first problem to be solved in order to improve the performance of these coatings under fast pulses. **Figure 18** shows the resistive heat density for the same case presented in **Figure 16**. It can be noticed that the heat is produced mainly in the CAT. The heat and electric field in the CAT can be reduced by increasing the conductivity of this coating; however, the high stress will be now moved to the SGT. A possible solution consists of controlling both the material properties and the designs of stress-grading system [26]. For example, a sectionalized stress-grading system consisting of two coatings with different conductive properties can be used in the CAT in addition to the SGT in order to divide the electric field and ohmic losses at the coil end. The first part, starting from the slot end, is a highly conductive coating, and the second part is now referred to as stress-grading coating for high-frequency components (SG_{HF}). The SG_{HF} coating is designed to filter and relieve the fast rise front of the pulses, while a third coating (SG_{LF}) is used to grade the lower frequency components of the PWM voltage waveform.

As an example, consider a sectionalized stress-grading system where the thickness of the SG_{HF} and SG_{LF} layers is duplicated (1 mm), and the electric properties of the first layer are conductivity of 0.5 S/m, and $\varepsilon_r = 50$, for the second conductive layer (SG_{HF}): conductivity of 0.05 S/m, and $\varepsilon_r = 50$. The third layer SGT is an with the same nonlinear characteristic given by Eq. (11), but with a value of $\sigma_0 = 1.85 \times 10^{-8}$ S/m.

The distribution of resistive heat and electric field is modified, as it can be seen in **Figure 19**. With the first conductive layer, the maximum heat is moved to the SG_{HF} and SG_{LF} layers and reduced in around 50%, see **Figure 19(a)**. The electric field is not increased in the SG_{LF} in comparison with the electric field in the original design presented in **Figure 16**, as shown in **Figure 19(b)**. This is an example of how modeling allows modifying the properties and dimensions of the stress-grading coatings in order to obtain the desired stress grading.

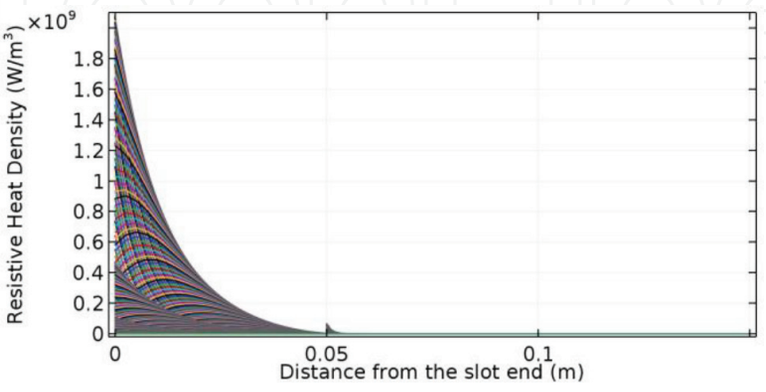

Figure 18. Resistive heat distribution along the stress-grading coatings for the same case of the results presented in **Figure 14**.

http://dx.doi.org/10.5772/intechopen.78064

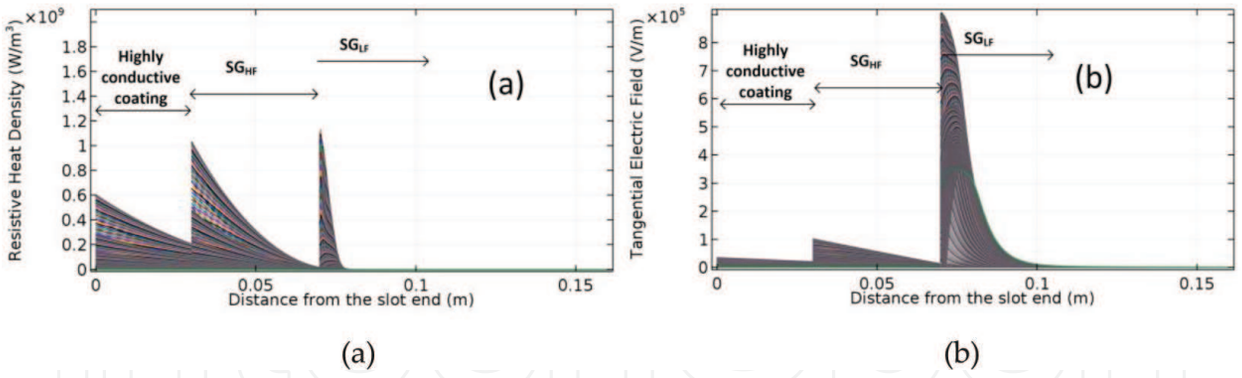

Figure 19. (a) Resistive heat and (b) electric field distribution along the sectionalized stress-grading system.

3.4. Simulation of the tapping of stress-grading systems under fast pulses

As mentioned before, an important characteristic of FEM modeling of stress-grading systems is the possibility of taking into account some details of the geometry that can influence the stress distribution under fast rise time pulses. In tape-based SG systems, the SGT usually overlaps the CAT a couple of centimeters, with one or two full-lapped turns followed by half-lapped turns until it reaches the desired length. During FEM modeling, the overlapping interfaces can be reproduced as in the real condition; however, it is not usual to consider the tape interfaces. Optical micrographs of the overlapping tape sections, obtained from form-wound coils, have shown that there are transition sections of the coatings with only one tape thickness between segments with two tape thickness [54].

Two-dimensional FEM simulations of the stress-grading system are performed considering the coatings configuration and the voltage waveform from **Figure 15**, but now the geometrical shape of the half overlapping between tape turns is included. For this case, the conductivity of the CAT was considered as 0.01 S/m, with a relative permittivity of 50,

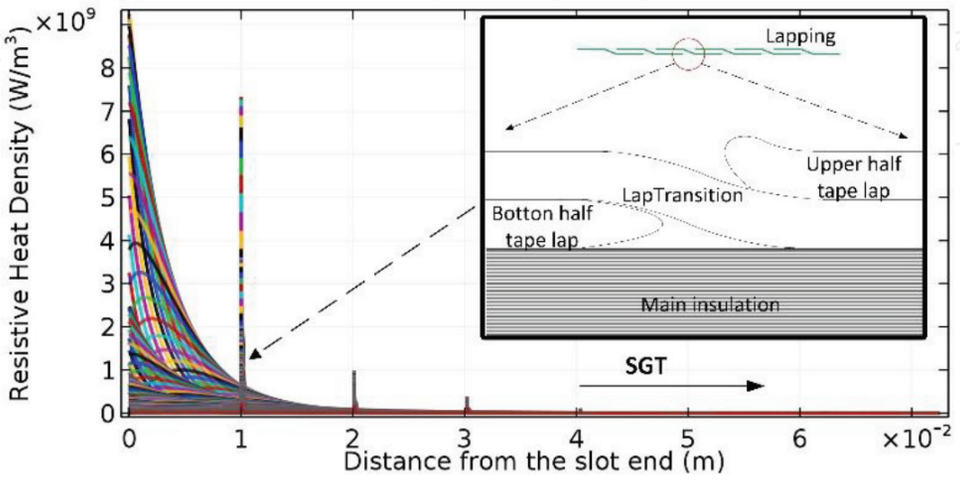

Figure 20. Heat in the CAT and SGT coatings considering the tape overlappings.

and the CAT-CAT overlappings occurring every centimeter. The conductivity of the SGT is given by Eq. (11). The shape considered for the tape overlappings is shown in the inset of **Figure 20**. In the same figure, the simulation results show how the CAT-CAT overlappings present high values of heat, behavior that is experimentally confirmed by the temperature distribution presented in **Figure 14**. These results demonstrate how the quality of the application of these tape-based coatings must be guaranteed to avoid early problems with the machines fed by PWM drives.

4. Conclusions

Two crucial topics for the proper insulation design of MV motors excited by PWM drives have been reviewed in this chapter: modeling of the windings for pulse propagation analysis and modeling of the stress-grading system.

A frequency domain non-uniform multi-conductor transmission line approach has been used to study the fast-front transient response of a machine-winding coil when a PWM-type excitation from an inverter is applied. The parameters of the coil were calculated using the finite-element method. The results when applying a PWM-type excitation to the coil show that the rise time of the source and the length of the cable has an important effect on the transient overvoltage produced at different turns of the coil, as well as in the potential difference between adjacent turns. The comparison between simulation and experimental results, in terms of oscillatory behavior and magnitude, demonstrates that both the winding model and the cable model selected result in a very accurate prediction of the fast-transient response related to the use of inverters in medium-voltage induction machines. Since the winding model is considered as linear for high frequencies, a frequency domain-modeling approach is a very good option to study the fast-transient response of machine windings.

On the other hand, the conductive armor and semi-conductive-grading coatings are important parts of the insulation system in rotating machines. The correct design of these coatings becomes difficult when PWM voltages feed the machine from adjustable speed drives. The stress-grading coatings often cannot effectively relieve the stress during repetitive surge voltages and, in the extreme case, hot spots and/or PDs will gradually destroy the coatings, making the problem worse. FEM modeling is a useful tool in understanding the influence of the various design parameters eliminating the trial and error methods that usually require more time and other resources. By reducing the dimension of the elements used to discretize the stress-grading coatings subdomains, it is possible to reduce the computational burden, but when a detailed geometry of the stress-grading system needs to be included in the simulation, this option cannot be considered. By using FEM modeling, it is possible to compute the maximum electric field, power loss, or voltage at the end of the SGT and use these variables in conjunction with optimization subroutines to obtain improved designs.

Author details

Fermin P. Espino Cortes[1], Pablo Gomez[2]* and Mohammed Khalil Hussain[2,3]

*Address all correspondence to: pablo.gomez@wmich.edu

1 Instituto Politecnico Nacional, Mexico City, Mexico

2 Western Michigan University, Kalamazoo, MI, USA

3 University of Baghdad, Baghdad, Iraq

References

[1] Calvert JF. Protecting machines from line surges. Transactions of the American Institute of Electrical Engineers. 1934;**53**(1):139-146

[2] Abetti PA, Maginniss FJ. Fundamental oscillations of coils and windings. Transactions of American Institute of Electrical Engineers. Part III: Power Apparatus and Systems. 1954; **73**(1):1-10

[3] Cornick KJ, Thompson TR. Steep-fronted switching voltage transients and their distribution in motor windings. Part 2: Distribution of steep-fronted switching voltage transients in motor windings. IEE Proceedings B – Electric Power Applications. 1982;**129**(2):56-63

[4] Oraee H, McLaren PG. Surge voltage distribution in line-end coils of induction motors. IEEE Transactions on Power Apparatus and Systems. 1985;**PAS-104**(7):1843-1848

[5] Guardado JL, Cornick KJ. A computer model for calculating steep-fronted surge distribution in machine windings. IEEE Transactions on Energy Conversion. 1989;**4**(1):95-101

[6] Guardado JL, Cornick KJ, Venegas V, Naredo JL, Melgoza E. A three-phase model for surge distribution studies in electrical machines. IEEE Transactions on Energy Conversion. 1997;**12**(1):24-31

[7] Su CQ, editor. Electromagnetic Transients in Transformer and Rotating Machine Windings. 1st ed. Hersey: IGI Global; 2013

[8] Stranges MKW, Stone GC, Bogh DL. Progress on IEC 60034-18-42 for qualification of stator insulation for medium-voltage inverter duty applications. In: Proceedings of IEEE Petroleum and Chemical Industry Technical Conference (PCIC'07); 17–19 Sept. 2007; Calgary, Canada. US: IEEE; 2007. pp. 1-7

[9] Stone GC, Culbert I. Review of stator insulation problems in medium voltage motors fed from voltage source PWM drives. In: Proceedings of International Symposium on Electrical Insulating Materials (ISEIM'14); 1–5 June 2014; Niigata, Japan. US: IEEE; 2014. pp. 50-53

[10] He J, Sizov GY, Zhang P, Demerdash NAO. A review of mitigation methods for overvoltage in long-cable-fed PWM AC drives. In: Proceedings of IEEE Energy Conversion Congress and Exposition (ECCE'11); 17–22 Sept 2011; Phoenix, AZ. US: IEEE; 2011. pp. 2160-2166

[11] Nussbaumer P, Mitteregger A, Wolbank TM. Online detection of insulation degradation in inverter fed drive systems based on high frequency current sampling. In: Proceedings of 37th Annual Conference on IEEE Industrial Electronics Society (IECON'11); 7–10 Nov. 2011; Melbourne, Australia. US: IEEE; 2012. pp. 1954-1959

[12] Moreira FS, D'Angelo MFSV, Palhares RM, Caminhas WM. Incipient fault detection in induction machine stator-winding using a fuzzy-Bayesian two change points detection approach. In: Proceedings of 9th IEEE/IAS International Conference on Industry Applications (INDUSCON); 8–10 Nov. 2010; Sao Paulo, Brazil. US: IEEE;2011. pp. 1-6

[13] Gandhi A, Corrigan T, Parsa L. Recent advances in modeling and online detection of stator interturn faults in electrical motors. IEEE Transactions on Industrial Electronics. 2011; **58**(5):1564-1575

[14] Refaat SS, Abu-Rub H, Saad MS, Aboul-Zahab EM, Iqbal A. Detection, diagnoses and discrimination of stator turn to turn fault and unbalanced supply voltage fault for three phase induction motors. In: Proceedings of IEEE International Conference on Power and Energy (PECon); 2–5 Dec. 2012; Kota Kinabalu, Malaysia. US: IEEE; 2013. pp. 910-915

[15] Nussbaumer P, Vogelsberger MA, Wolbank TM. Induction machine insulation health state monitoring based on online switching transient exploitation. IEEE Transactions on Industrial Electronics. 2015;**62**(3):1835-1845

[16] Chaturvedi DK, Iqbal MS, Singh MP. Health monitoring techniques of induction motor: An overview. In: Proceedings of the International Conference on Emerging Trends in Engineering& Technology; 25–27 Oct. 2013; Kurukshetra, India. Netherlands: ACEEE; 2013. pp. 469-477

[17] Fabiani D, Cavallini A, Montanari GC. Aging investigation of motor winding insulation subjected to PWM-supply through PD measurements. In: Annual Report Conference on Electrical Insulation and Dielectric Phenomena (CEIDP), 16–19 Oct., Nashville, TN. USA: IEEE; 2005. pp. 434-437

[18] Greenwood A. Electrical Transients in Power Systems. 2nd ed. New York: Wiley; 1991

[19] Rudenberg R. Performance of traveling waves in coils and windings. Electrical Engineering. 1940;**59**(12):1031-1040

[20] Rabins L. A new approach to the analysis of impulse voltages and gradients in transformer windings. Transactions of American Institute of Electrical Engineers. 1960;**79**(4): 1784-1791

[21] Hussain MK, Gomez P. Modeling of machine coils under fast front excitation using a non-uniform multiconductor transmission line approach. In: Proc. of North American Power Symposium (NAPS'16); 18–20 Sept. 2016; Denver, CO. US: IEEE; 2016. pp. 1-6

[22] de León F, Gomez P, Martinez-Velasco JA, Rioual M. Transformers. In: Martinez-Velasco JA, Editor. Power System Transients: Parameter Determination. 1st ed. Boca Raton: CRC Press. pp. 177-250

[23] Stone GC, Boulter EA, Culbert I, Dhirani H. Electrical Insulation for Rotating Machines, Design, Evaluation, Aging, Testing, and Repair. 2nd ed. Hoboken: Wiley - IEEE Press; 2014

[24] Haque SM, Ardila-Rey JA, Masud AA, Umar Y, Albarracín R. Electrical properties of different polymeric materials and their applications: The influence of electric field. In: Boxue D, editor. Properties and Applications of Polymer Dielectrics. Rijeka, Croatia: InTech; 2017 Chapter 3

[25] Kielmann F, Speck J. Behaviour of the stress grading systems in converter operated H.V. Machines. In: Proceedings of 10th International Insulation Conference (INSUCON); 24–26 May 2006; Birmingham, UK. US: IEEE; 2006. pp. 99-104

[26] Espino-Cortes FP, Cherney EA, Jayaram SH. Impact of inverter drives employing fast switching devices on form-wound AC machine stator coil stress grading. IEEE Electrical Insulation Magazine. 2007;**23**(1):16-28

[27] Luna Z, Gómez P, Espino-Cortes FP, Peña R. Modeling of transformer windings for fast transient studies: Experimental validation and performance comparison. IEEE Transactions on Power Delivery. August 2017;**32**(4):1852-1860

[28] Gómez P, Uribe FA. The numerical Laplace transform: An accurate technique for analyzing electromagnetic transients on power system devices. International Journal of Electrical Power & Energy Systems. 2009;**31**(2):116-123

[29] COMSOL. Introduction to COMSOL Multiphysics 5.3a [Internet]. 2017. Available from: https://cdn.comsol.com/documentation/5.3.1.180/IntroductionToCOMSOLMultiphysics.pdf [Accessed: February 09, 2018]

[30] Gomez P, Moreno P, Naredo JL. Frequency-domain transient analysis of nonuniform lines with incident field excitation. IEEE Transactions on Power Delivery. 2005;**20**(3):2273-2280

[31] Moreno P, Gomez P, Davila M, Naredo JL. A uniform line model for non-uniform single-phase lines with frequency dependent electrical parameters. In: Proceedings of IEEE Transmission & Distribution Conference and Exposition; 15–18 Aug 2006; Caracas, Venezuela. US: IEEE; 2007. pp. 1-6

[32] Gomez P, Escamilla JC. Frequency domain modeling of nonuniform multiconductor lines excited by indirect lightning. International Journal of Electrical Power & Energy Systems. 2013;**45**(1):420-426

[33] Nuricumbo-Guillen R, Gomez P, Espino-Cortes FP. Computation of transient voltage profiles along transmission lines by successive application of the numerical Laplace transform. In: Proceedings of North American Power Symposium (NAPS); 22–24 Sept 2013; Manhattan, KS. US: IEEE; 2013. pp. 1-6

[34] Ul Haq S, Stranges MKW, Wood B. A proposed method for establishing partial discharge acceptance limits on API 541 and 546 sacrificial test coils. IEEE Transactions on Industry Applications. 2017;**53**(1):718-722

[35] Hussain MK, Gomez P. Modeling and experimental analysis of the transient Overvoltages on machine windings fed by PWM inverters. In: Proceedings of International Conference on Power System Transients; 26–29 June. Vol. 2017. South Korea: Seoul; 2017. pp. 1-6

[36] Rivenc JP, Lebey T, Loubiere A, Biron M, Warnant J. A discussion of current-voltage and surface potential measurements to test stress grading materials. J. Physics D: Appl. Phys. 1998;**31**:2612-2621

[37] Staubach C, Hildinger T, Staubach A. Comprehensive electrical and thermal analysis of the stress grading system of a large hydro generator. IEEE Electrical Insulation Magazine. 2018;**34**(1):37-49

[38] Kone G, Volat C. Numerical investigation of transient potential distribution along stress-grading on stators bars (Roebel type). IEEE Electrical Insulation Conference (EIC), Montreal, QC, CA: IEEE. 2016;**2016**:9-12

[39] Umemoto T, Tsurimoto T, Kisakibaru T, Sakurai T, Tsuda T, Karasawa K. Novel evaluation methods of end-turn stress grading materials for converter-fed high voltage rotating machines. Conference on Electrical Insulation and Dielectric Phenomena (CEIDP), Toronto, ON, CA: IEEE. 2016:307-310

[40] Zhang L, Calebrese C. Karakus Y, Dickens K, Yin W. Inverter fed motor stress grading system design consideration. 13th International Electrical Insulation Conference (INSUCON), Birmingham, UK. 2017:1-5

[41] Sharifi E, Jayaram SH, Cherney EA. Temperature and electric field dependence of stress grading on form-wound motor coils. IEEE Transactions on Dielectrics and Electrical Insulation. 2010;**17**(1):264-270

[42] Egiziano L, Tucci V, Petrarca C, Vitelli M. A Galerkin model to study the field distribution in electrical components employing nonlinear stress grading materials. IEEE Transactions on dielectrics and electrical insulation. 1999;**6**(6):765-773

[43] Bayon L, Buret F, Koelblin C, Toledo T. Field distribution measurement and simulation of stress control materials for cable accessories. In: Proceedings of the 2004 IEEE International Conference on Solid Dielectrics ICSD 2004, Toulouse, France. 2004, 2. pp. 534-537

[44] Allison JA. Understanding the need for anti-corona materials in high voltage rotating machines. In: Proceedings of 6th International Conference on Properties and Applications of Dielectric Materials; 21–26 June 2000; Xi'an, China. US: IEEE; 2002. pp. 860-863

[45] Nam NN, Matsumoto S. Electrical and thermal computation of stress grading system in inverter-driven medium voltage motors. IEEJ Transactions on Fundamentals and Materials. 2013;**133**(11):591-597

[46] Kumada A, Nakamura T, Ikeda H, Hidaka K, Tsuboi Y, Kisakibaru T, Yoshimitsu T. Transient potential distribution on stress grading system of rotating machines under repetitive impulse voltages. In: Proceedings of Electrical Insulation Conference (EIC); 8–11 June 2014; Philadelphia, PA. US: IEEE; 2014. pp. 368-372

[47] Baker AE, Gully AM, Wheeler JCG. Finite element modeling of non-linear stress grading materials for machine end windings. In: Proceedings of IEE Conference on Power Electronics, Machines and Drivers; 4–7 June 2002; Santa Fe, NM. US: IEEE; 2002. pp. 265-268

[48] Yeo Z, Buret F, Krahenbuhl L, Auriol P. A nonlinear model for surface conduction. IEEE Transactions on Magnetics. 1998;**34**(5):2617-2620

[49] Wheeler JCG, Gully AM, Baker AE, Perrot FA. Novel stress grading systems for converter-fed motors. IEEE Electrical Insulation Magazine. 2007;**23**(1):29-35

[50] Espino-Cortés FP, Gómez P, Betanzos Ramírez D. Modeling of the heat generation on stress grading coatings of motors fed by multilevel drives. IEEE Transactions on Dielectrics and Electrical Insulation. 2011;**18**(4):1328-1333

[51] Sharifi E, Fink H. Slot corona protection systems for medium voltage rotor windings subjected to PWM voltage in doubly fed induction generators. In: Proceedings of Electrical Insulation Conference (EIC); 8–11 June 2014; Philadelphia, PA. US: IEEE; 2014. pp. 378-381

[52] Chen W, Gao G. Using multi-stress aging test to evaluate and improve medium-voltage stator insulation for adjustable speed drive applications. In: In: Proceedings of IEEE Petroleum and Chemical Industry Technical Conference (PCIC'11); 19–21 Sept. Vol. 2011. Toronto, Canada. US: IEEE; 2011. pp. 1-7

[53] Espino-Cortés FP, Asiain-Olivares TI, Gómez P. Simulation of the effect of armor coating conductivity on the stress grading coating performance under PWM multilevel waveforms. Electrical Insulation Conference (EIC), Seattle, Washington, USA: IEEE; 7–10 June. 2015;**2015**:172-175

[54] Ramirez-Serrano JC, Espino-Cortes FP, Hernandez-Ramirez EJ. Electric field and heat at the CAT-SG coatings interface under fast rise pulses. In: Proceedings of electrical insulation conference (EIC); 17-20 June 2018; San Antonio TX. US: IEEE; to be published

IntechOpen